

# Gluon shadowing effects on $J/\psi$ and $\Upsilon$ production in $p+\text{Pb}$ collisions at $\sqrt{s_{NN}} = 115$ GeV and $\text{Pb}+p$ collisions at $\sqrt{s_{NN}} = 72$ GeV at AFTER@LHC

R. Vogt<sup>1,\*</sup>

<sup>1</sup>*Nuclear and Chemical Sciences Division, Lawrence Livermore National Laboratory, Livermore, CA 94551, USA  
Physics Department, University of California at Davis, Davis, CA 95616, USA*

We explore the effects of shadowing on inclusive  $J/\psi$  and  $\Upsilon(1S)$  production at AFTER@LHC. We also present the rates as a function of  $p_T$  and rapidity for  $p+\text{Pb}$  and  $\text{Pb}+p$  collisions in the proposed AFTER@LHC rapidity acceptance.

Keywords: quarkonium, cold nuclear matter effects

## I. INTRODUCTION

The AFTER@LHC quarkonium program has the unique opportunity to study quarkonium production at large momentum fractions,  $x$ , in the target region [1]. The most favorable configuration for high rates at large  $x$  for the nucleus is a proton beam from the LHC on a heavy nuclear target. In this case, the nucleon-nucleon center of mass energy is more than half that of the RHIC collider,  $\sqrt{s_{NN}} = 115$  GeV, for the top LHC proton beam energy of 7 TeV. However, the fixed-target configuration is an advantage because of the higher intensity on target. The longer LHC proton runs gives a luminosity over a  $10^7$  s LHC 'year'. On a 1 cm thick Pb target, with  $p+\text{Pb}$  collisions,  $\mathcal{L} = 16A \mu\text{b}^{-1} \text{s}^{-1}$ . When a lead beam is extracted the run time is shorter, an LHC Pb 'year' is  $10^6$  s. The lower  $Z/A$  ratio also results in a lower center-of-mass energy of  $\sqrt{s_{NN}} = 72$  GeV for the top lead beam energy of 2.76 TeV. On a liquid  $\text{H}_2$  target, for  $\text{Pb}+p$  collisions,  $\mathcal{L} = 8A_{\text{Pb}} \text{mb}^{-1} \text{s}^{-1}$  per centimeter target length so that a 1 m target gives a luminosity of  $\mathcal{L} = 800A_{\text{Pb}} \text{mb}^{-1} \text{s}^{-1}$  [1].

Here we will consider the inclusive  $J/\psi$  and  $\Upsilon(1S)$  rates in  $p+\text{Pb}$  collisions at  $\sqrt{s_{NN}} = 115$  GeV and  $\text{Pb}+p$  collisions at  $\sqrt{s_{NN}} = 72$  GeV. The results are presented as a function of rapidity,  $y$ , and transverse momentum,  $p_T$ , of the quarkonium state. We choose to present the  $p_T$  results in a 0.5 unit wide rapidity bin in the backward region of the center of mass of the collision,  $-2.5 < y_{\text{cms}} < -2.0$  for  $\sqrt{s_{NN}} = 115$  GeV and  $-1.9 < y_{\text{cms}} < -1.4$  for  $\sqrt{s_{NN}} = 72$  GeV. This is a region that has been virtually unexplored in previous quarkonium production measurements but, as we will show, can be studied by AFTER@LHC with relatively high statistics in most cases.

Our calculations are done in the next-to-leading order (NLO) color evaporation model (CEM) [2] and employ

the EPS09 NLO parameterization [3] of the effects of modification of the parton distribution functions in the nucleus, referred to here as 'shadowing'. Since this set also provides an uncertainty band, the results are representative of the range of shadowing parameterizations produced by other groups.

We also present the nuclear suppression factor ratios,  $R_{p\text{Pb}}$  for  $p+\text{Pb}$  collisions and  $R_{\text{Pb}p}$  for  $\text{Pb}+p$  collisions. These quantities are the ratio of the per nucleon cross sections in  $p+\text{Pb}$  ( $\text{Pb}+p$ ) collisions relative the same cross section in  $p+p$  collisions at the same center of mass energy. These ratios are also given as a function of  $p_T$  and  $y$ .

In Sec. II, we will show the EPS09 NLO shadowing parameterizations at the appropriate factorization scale for  $J/\psi$  and  $\Upsilon$  production as a function of  $x$  with emphasis on the appropriate  $x$  regions for the AFTER@LHC kinematics. We present the ratios and rates obtained with the EPS09 NLO parameterization in Sec. III. We conclude with some final remarks in Sec. IV.

## II. SHADOWING PARAMETERIZATION

Our calculations employ the EPS09 shadowing parameterization [3]. At NLO, it is based on the CTEQ6M proton parton densities (PDFs) [4]. In our calculations of quarkonium production [5, 6], we use the CT10 [7] proton PDFs with the EPS09 NLO parameterization. As long as both calculations are at NLO, the choice of proton PDFs used to calculate quarkonium production does not affect the shape or magnitude of the nuclear suppression factors [8].

One possibility for the AFTER@LHC experiment is to use the LHCb detector, either as is, with  $2 < y_{\text{lab}} < 5$ , or an improved LHCb (LHCb+), with  $1 < y_{\text{lab}} < 5$ .

In the fixed-target kinematics of AFTER@LHC, with a 7 TeV proton beam, the rapidity range is  $\Delta y = 4.8$ , corresponding to a center of mass rapidity coverage of  $-2.8 < y_{\text{cms}} < 0.2$  for LHCb or  $-3.8 < y_{\text{cms}} < 0.2$  for LHCb+ in  $p+\text{Pb}$  collisions at  $\sqrt{s_{NN}} = 115$  GeV. In this

\* vogt2@llnl.gov

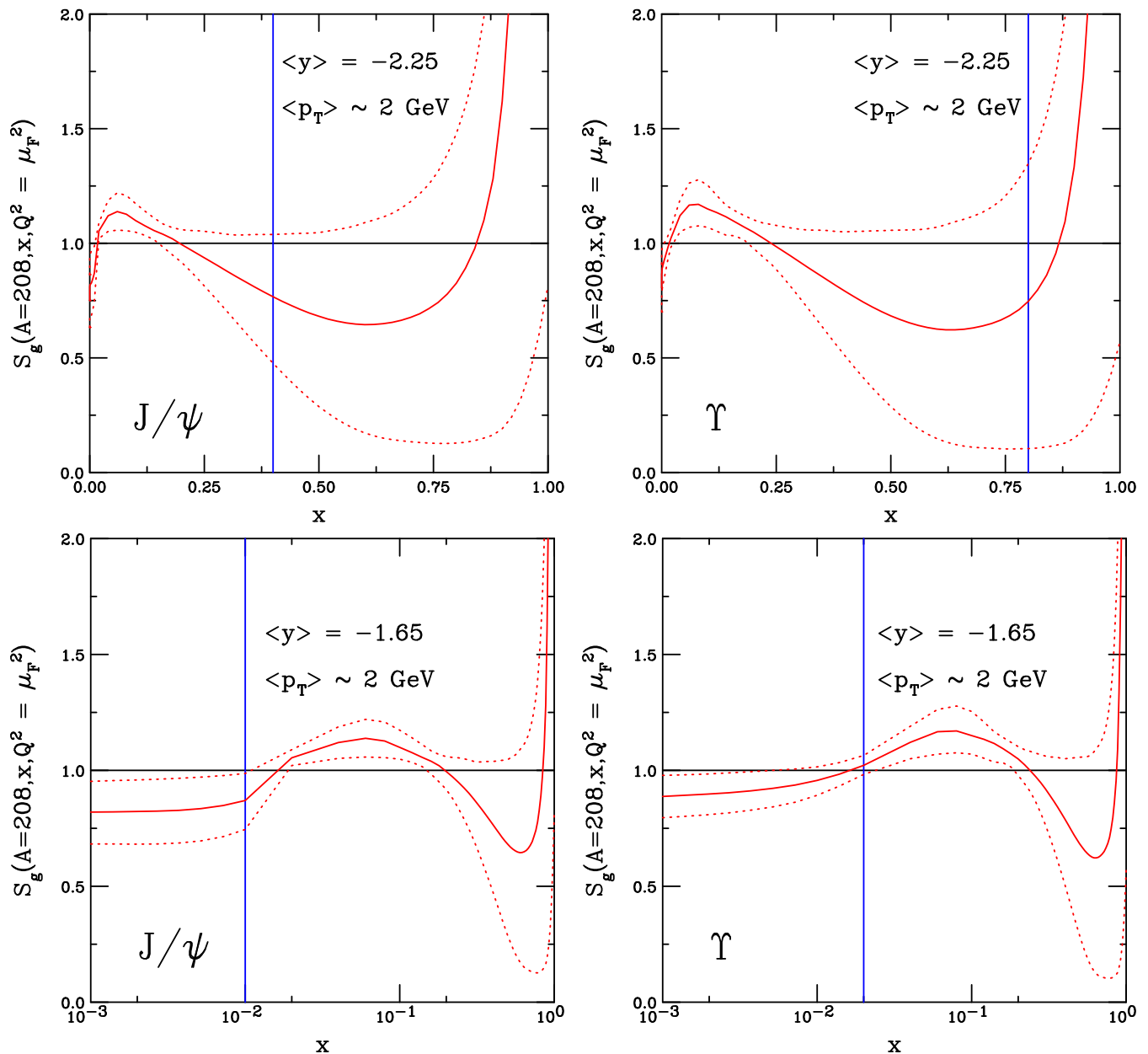


Figure 1: The EPS09 NLO shadowing ratios for  $J/\psi$  (left) and  $\Upsilon(1S)$  (right) production. The solid curve in each plot is the central EPS09 NLO result while the dotted curves outline the shadowing uncertainty band. The upper plots are on a linear scale to emphasize the large  $x$  region while the lower ones are on a logarithmic scale to expand the low  $x$  region. The approximate kinematic area of interest is indicated by the vertical line in each case.

case, the Pb nucleus is the target. If  $x_1$  refers to the momentum fraction probed in the proton beam and  $x_2$  is the momentum fraction probed in the lead target, in these kinematics, the negative rapidity means that  $x_2$  is large,  $x_2 > 0.1$ . This  $x_2$  range has not been explored since early nuclear deep-inelastic scattering (nDIS) measurements such as by the European Muon Collaboration [9] and at SLAC [10] and has never been explored by gluon-dominated processes such as quarkonium production. AFTER@LHC would be the first experiment to

probe these kinematics since most fixed-target configurations studying quarkonium have placed the detectors downstream where  $x_1 > x_2$ , as at the CERN SPS [11, 12] and the Fermilab Tevatron [13]. The only quarkonium experiment to measure part of this backward, large  $x_2$  region was HERA-B with its foils placed around the edges of the proton beam at HERA [14].

On the other hand, with a 2.76 TeV lead beam, the rapidity range is  $\Delta y = 4.3$ , corresponding to a center of mass rapidity coverage of  $-2.3 < y_{\text{cms}} < 0.7$  for LHCb

or  $-3.3 < y_{\text{cms}} < 0.7$  for LHCb+ in Pb+ $p$  collisions at  $\sqrt{s_{NN}} = 72$  GeV. In this case, the proton is the target, with  $x_2$ , and the lead beam is assigned  $x_1$ . Thus, the nuclear momentum fractions probed are moderate,  $x_1 \sim 0.01$ . This  $x$  region has been well studied in nDIS experiments but, again, not for final states dominated by initial-state gluons.

Global fits to the nuclear parton densities (nPDFs), such as EPS09, typically include nuclear deep-inelastic scattering data ( $F_2$  in  $l + A$  and  $dF_2/d \ln Q^2$ ), Drell-Yan data, and, more recently, RHIC data such as  $\pi^0$  production [3]. The range over which DGLAP evolution can be applied ( $Q^2 > 1 \text{ GeV}^2$ ) for fixed-target nDIS limits the minimum  $x$  values probed. In addition, such analyses do not take into account the possibility of any other cold nuclear matter effects so that the possibility of an effect such as initial-state energy loss in matter by quarks in Drell-Yan dilepton production is folded in with the global analysis of nuclear shadowing. Quarkonium production is particularly subject to other cold nuclear matter effects such as energy loss in matter, break up of the quarkonium state by nucleons (nuclear absorption), and interactions with comoving hadrons, see e.g. Ref. [15] for a discussion. For the purposes of this paper, we focus only on the expected effects of shadowing.

Figure 1 shows the EPS09 NLO gluon shadowing parameterization as a function of momentum fraction,  $x$ . The scales at which the results are shown correspond to those used in the CEM for  $J/\psi$  (left-hand side) and  $\Upsilon$  (right-hand side) production. Along with the central set, denoted by the solid curves, the dotted curves display the uncertainty band. EPS09 obtains 30 additional sets of shadowing ratios by varying each of the 15 parameters within one standard deviation of the mean. The differences are added in quadrature to produce the uncertainty band in the shadowing ratio  $S_g$ . (We note that the uncertainties in the corresponding LO set are larger while the central shadowing effect is greater at LO than at NLO. For more details concerning this set as well as differences between other available nPDF sets, see Ref. [8].)

The vertical blue line in each panel shows the average  $x$  value for the final quarkonium states at each energy,  $p$ +Pb on top and Pb+ $p$  on the bottom. This is obtained by estimating the average  $x$  value from the simpler  $2 \rightarrow 1$  kinematics of the LO CEM with  $x_{1,2} = (2m/\sqrt{s_{NN}}) \exp(\pm y)$  and replacing  $m$  by  $m_T = \sqrt{m^2 + p_T^2}$  with  $p_T^2 = 0.5(p_{T_Q}^2 + p_{T_{\bar{Q}}}^2)$ . The  $x$  value from the LO CEM represents a lower limit on  $x$  relative to the actual  $2 \rightarrow 2$  and  $2 \rightarrow 3$  kinematics of the LO and NLO contributions to the full NLO CEM calculation. The average center of mass rapidity,  $\langle y_{\text{cms}} \rangle$ , shown on each panel is the approximate midpoint of our chosen rapidity interval in each case. The average  $p_T$  of  $\sim 2$  GeV is near the peak of the  $p_T$  distributions. These values should not be thought of as having the most weight in the actual calculations which integrate over the rapidity interval for the  $p_T$  distributions and all  $p_T$  for the rapidity distributions. Indeed, since the rapidity distributions are steeply

falling, the preponderance of the rate comes from the upper end of the range in each case. Thus the vertical lines represent an estimate of the lower bound on the  $x$  range at the given value of  $p_T$ .

The  $p$ +Pb kinematics emphasize high  $x$  in the nucleus (top panels) and thus explores an  $x$  range rarely probed, especially by gluon-dominated processes. It is partly in the 'EMC' region of the  $x$  range and also moves into the regime of 'Fermi motion', see a discussion of how the various  $x$  regions are parameterized by Eskola and collaborators in Refs. [16, 17]. Given the shortage of direct gluon-induced data in the global analyses, the gluon shadowing ratios are constrained by the momentum sum rule. The gluon shadowing ratios shown in the top half of Fig. 1 are plotted on a linear scale to highlight the large  $x$  region. Here the scale dependence is very weak, illustrated by the similarities in the results for the two quarkonium scales shown, while the uncertainties in the nPDF extraction are the largest. AFTER@LHC measurements could help narrow this uncertainty range.

On the other hand, the Pb+ $p$  kinematics are in an  $x$  region where quark-dominated processes, as in nDIS, are well measured and the uncertainties can be expected to be relatively small.

### III. COLD NUCLEAR MATTER EFFECTS AND QUARKONIUM PRODUCTION RATES

There are other possible cold matter effects on  $J/\psi$  production in addition to that of shadowing: breakup of the quarkonium state due to inelastic interactions with nucleons (absorption) or produced hadrons (comovers) and energy loss in cold matter.

The quarkonium absorption cross section at midrapidity was seen to decrease with center-of-mass energy in Ref. [18], independent of whether shadowing effects were included or not. It was also seen that incorporating shadowing into the extraction of the absorption cross section required a larger effective cross section [18]. Extrapolating from the results of Ref. [18] to the energy range of AFTER@LHC, we can expect an effective absorption cross section of a few millibarns at midrapidity. Away from midrapidity, the effective absorption cross section was seen to rise at forward Feynman  $x$ ,  $x_F$  [18], which could be attributed to energy loss in matter [19]. When a similar analysis was extended to the RHIC collider geometry, the effective absorption cross section was also seen to increase in the backward region [20]. Such behavior could be attributed to the quarkonium state being fully formed inside the nucleus. The  $p$ +Pb kinematics of AFTER@LHC would be an ideal environment to study absorption in the target if other observables can also probe shadowing effects to disentangle the two.

The shadowing results shown here are obtained in the color evaporation model (CEM) [21, 22] at next-to-leading order in the total cross section [2]. In the CEM, the quarkonium production cross section is some fraction,

$F_C$ , of all  $Q\bar{Q}$  pairs below the  $H\bar{H}$  threshold where  $H$  is the lowest mass heavy-flavor hadron,

$$\sigma_C^{\text{CEM}}(s) = F_C \sum_{i,j} \int_{4m^2}^{4m_H^2} ds \int dx_1 dx_2 f_i^p(x_1, \mu_F^2) f_j^p(x_2, \mu_F^2) \hat{\sigma}_{ij}(\hat{s}, \mu_F^2, \mu_R^2), \quad (1)$$

where  $ij = q\bar{q}$  or  $gg$  and  $\hat{\sigma}_{ij}(\hat{s})$  is the  $ij \rightarrow Q\bar{Q}$  subprocess cross section. The normalization factor  $F_C$  is fit to the forward (integrated over  $x_F > 0$ )  $J/\psi$  cross section data and the combined  $\Upsilon(nS)$  state data at midrapidity. We use the code of Ref. [23] with the mass cut implemented.

The same values of the central charm quark mass and scale parameters are employed as those found for open charm,  $m_c = 1.27 \pm 0.09$  GeV,  $\mu_F/m_c = 2.10_{-0.85}^{+2.55}$ , and  $\mu_R/m_c = 1.60_{-0.12}^{+0.11}$  [5]. The normalization  $F_C$  is obtained for the central set,  $(m_c, \mu_F/m_c, \mu_R/m_c) = (1.27 \text{ GeV}, 2.1, 1.6)$ . The calculations for the extent of the mass and scale uncertainties are multiplied by the same value of  $F_C$  to obtain the extent of the  $J/\psi$  uncertainty band [5]. These values reproduce the energy dependence of  $J/\psi$  production from fixed-target to collider energies. The resulting rapidity and  $p_T$  distributions also agree with the  $p + p$  data from RHIC and the LHC at  $\sqrt{s} = 200$  GeV and 7 TeV respectively [5].

We calculate  $\Upsilon$  production in the same manner, with the central result obtained for  $(m_b, \mu_F/m_b, \mu_R/m_b) = (4.65 \text{ GeV}, 1.4, 1.1)$  [6]. We have also found good agreement with the  $\sqrt{s}$ , and  $p_T$  distributions from previous measurements [6]. Unfortunately, the uncertainties from RHIC measurements are rather large and few data are available on the shape of the  $\Upsilon$  rapidity distributions.

To obtain the quarkonium  $p_T$  distributions at low  $p_T$ , intrinsic transverse momentum,  $k_T$ , smearing for quarkonium is included in the initial-state parton densities [24]. Since the MNR code cancels divergences numerically, instead of slowing the calculations by adding more integrations, the  $k_T$  kick is added in the final, rather than the initial, state [23]. The Gaussian function  $g_p(k_T) = \pi \langle k_T^2 \rangle_p^{-1} \exp(-k_T^2 / \langle k_T^2 \rangle_p)$  [25], multiplies the parton distribution functions for both hadrons, assuming the  $x$  and  $k_T$  dependencies in the initial partons completely factorize. If factorization applies, it does not matter whether the  $k_T$  dependence appears in the initial or final state if the kick is not too large. The effect of the intrinsic  $k_T$  on the shape of the  $J/\psi$   $p_T$  distribution can be expected to decrease as  $\sqrt{s}$  increases because the average  $p_T$  of the  $J/\psi$  also increases with energy. However, the value of  $\langle k_T^2 \rangle$  may increase with  $\sqrt{s}$ . We can check the energy dependence of  $\langle k_T^2 \rangle$  by the shape of the  $J/\psi$   $p_T$  distributions at central and forward rapidity at RHIC. We find that  $\langle k_T^2 \rangle = 1 + (1/12) \ln(\sqrt{s}/20) \approx 1.19$  GeV<sup>2</sup> at  $\sqrt{s} = 200$  GeV agrees well with the  $J/\psi$   $p_T$  distributions [5]. All the calculations are NLO in the total cross section and assume that the intrinsic  $k_T$  broadening is the same in  $p + p$  as in  $p + \text{Pb}$ . While the broadening is expected to increase in collisions with nuclei as projectile, target or both, the agreement of the  $J/\psi$   $p + \text{Pb}$  ratio

$R_{p\text{Pb}}(p_T)$  with the LHC data is better without any additional broadening [8]. Therefore we do not change the value here.

### A. $J/\psi$ and $\Upsilon$ (1S) production in $p + \text{Pb}$ collisions at $\sqrt{s_{NN}} = 115$ GeV

In this section, the results for  $J/\psi$  and  $\Upsilon$  shadowing in  $p + \text{Pb}$  collisions at  $\sqrt{s_{NN}} = 115$  GeV are presented. Figure 2 shows the results for  $J/\psi$  while Fig. 3 shows the  $\Upsilon$  results. In both cases, the left-hand side shows the ratios  $R_{p\text{Pb}}$  as a function of  $y$  (top) and  $p_T$  in the rapidity range  $-2.5 < y_{\text{cms}} < -2$  (bottom). The rates to dileptons in the rapidity acceptance, assuming a lead target, are shown on the right-hand side of the figures.

In the kinematics of this configuration, the large  $x_2$  in the nucleus puts the peak for Fermi motion at the most negative rapidities. (The full center-of-mass rapidity range for  $J/\psi$ 's produced at this energy is  $|y_{\text{cms}}| = \ln(\sqrt{s}/m) < 3.8$  for the mass and scale parameters appropriate for the CEM calculation.) The EMC region is in the  $J/\psi$  rapidity acceptance. There is a steep drop in  $R_{p\text{Pb}}(y_{\text{cms}})$  as  $y_{\text{cms}}$  decreases from  $-2$  to  $-2.5$ , changing the central value of  $R_{p\text{Pb}}(y_{\text{cms}})$  by  $\sim 30\%$  over the range. The decrease into the EMC region is more apparent as a function of  $p_T$  where the region is expanded for  $p_T < 10$  GeV. The large uncertainty in this  $x$  range, as emphasized in the upper plots of Fig. 1, is enhanced here.

The rates as a function of rapidity for  $J/\psi$  and  $\Upsilon(1S)$  decays to lepton pairs are shown in Table I. While the rates are shown for the entire rapidity range, the broad LHCb+ center of mass rapidity acceptance ends at  $y_{\text{cms}} \sim 1$ . The rates are given in bins of  $\Delta y_{\text{cms}} = 0.5$  with the value of  $y_{\text{cms}}$  at the center of the bin shown in Table I. The rates include the branching ratios to lepton pairs.

The  $J/\psi$  rates in  $p + \text{Pb}$  collisions are very high. The rate is  $BdN/dy \sim 2.7 \times 10^8$  in the chosen backward rapidity bin of  $-2.5 < y_{\text{cms}} < -2$ , see the upper right panel of Fig. 2. The cross section is rather high since  $\sqrt{s_{NN}}$  is above the region where the production cross section is still increasing steeply with  $\sqrt{s_{NN}}$ . In addition, the  $J/\psi$  production range in rapidity is fully within the AFTER@LHC acceptance.

Finally, even though the rates fall off quickly with  $p_T$ , more than 100 events can be collected at  $p_T \sim 9.5$  GeV, see the lower right panel of Fig. 2 and the upper part of Table II, likely enough to determine where  $R_{p\text{Pb}}(p_T)$  lies within the EPS09 band.

The  $\Upsilon(1S)$  rates, shown in Fig. 3, are significantly lower. At this energy, the production cross section is still increasing rapidly so that the available phase space for  $\Upsilon$  production,  $|y_{\text{cms}}| < 2.9$  in the CEM calculation. Thus the AFTER@LHC acceptance is just inside the lower end of this range and the rate for  $\Upsilon$  production in this region is relatively low. While the rates over all

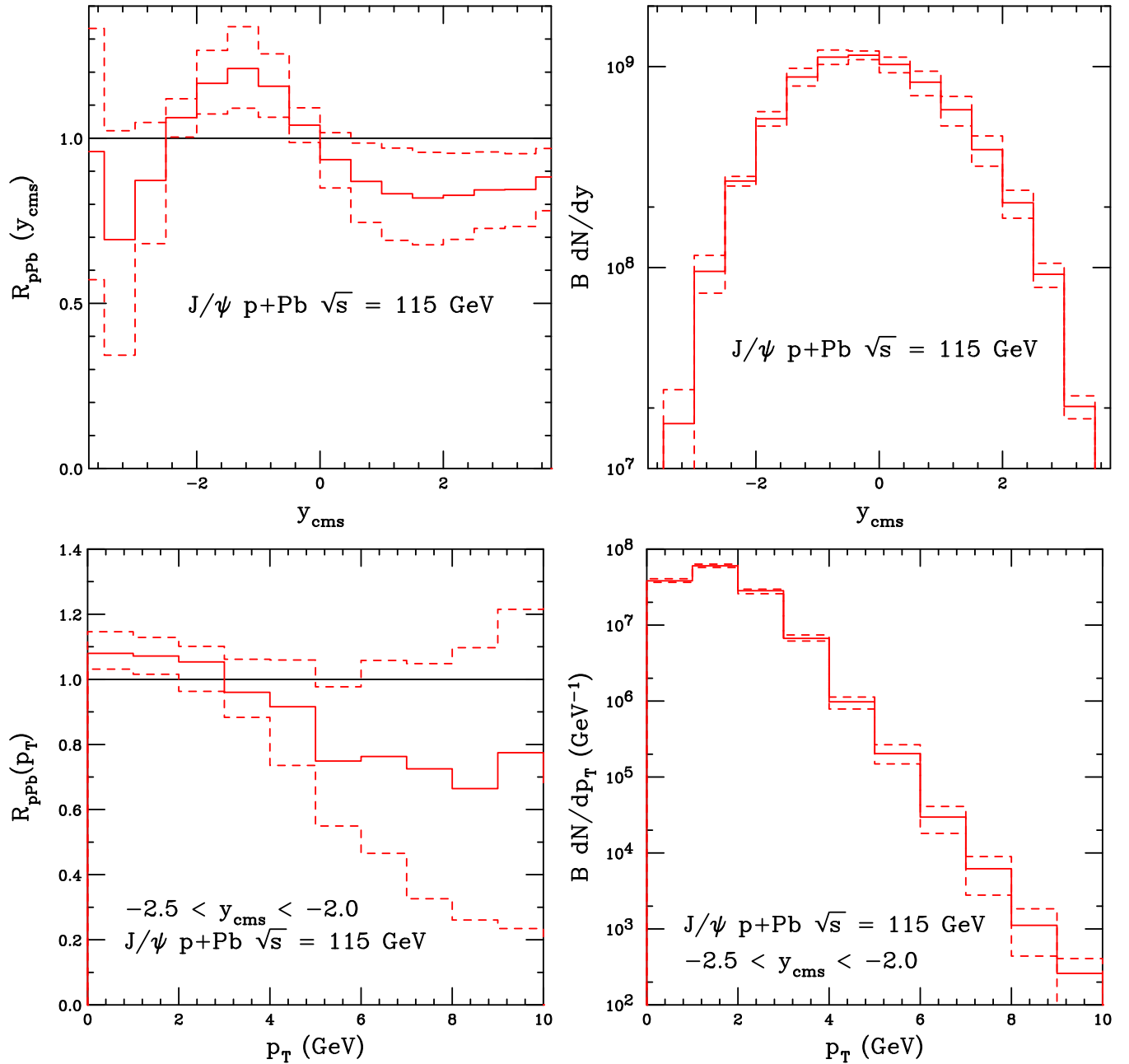


Figure 2: The predicted  $J/\psi$  shadowing ratios (left) and rates (right) as a function of center of mass rapidity (top) and  $p_T$  (bottom) for  $p+\text{Pb}$  collisions at  $\sqrt{s_{NN}} = 115$  GeV. The solid curve in each plot is the central EPS09 NLO result while the dotted curves outline the shadowing uncertainty band.

phase space can be quite high, with nearly  $10^6$  events at midrapidity, there are less than  $10^4$  events in the region  $-2.5 < y_{\text{cms}} < -2$ , see Table I and the lower right panel of Fig. 3.

As shown in Table II, the  $\Upsilon$  states that are produced in the AFTER@LHC acceptance are primarily at low  $p_T$ ,  $p_T \leq 3$  GeV. Indeed, there are fewer than 10 events per year for  $p_T > 6$  GeV so that any division into  $p_T$  bins for  $p_T > 5$  GeV is unlikely to be feasible.

The AFTER@LHC rapidity bin is in the EMC region and touching on the Fermi motion region at  $y_{\text{cms}} \sim -2.5$ , as seen on the upper left panel of Fig. 3. The  $p_T$  dependent ratio reflects the large uncertainty of the EMC region and is almost independent of  $p_T$  until  $p_T \sim 9$  GeV in the EPS09 parameterization where it increases sharply. The low rate will make it difficult to study this interesting region in detail.

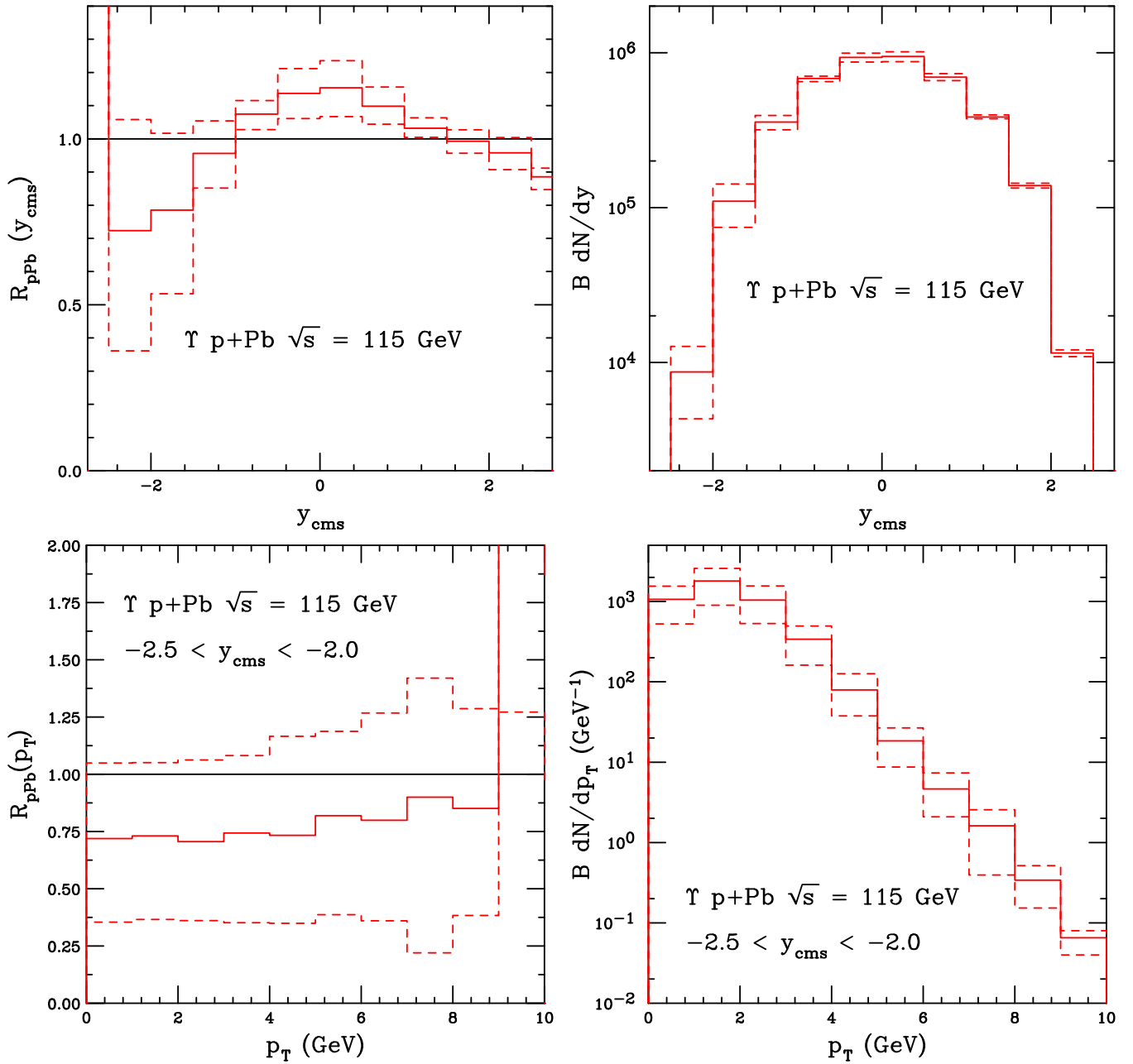


Figure 3: The predicted  $\Upsilon(1S)$  shadowing ratios (left) and rates (right) as a function of center of mass rapidity (top) and  $p_T$  (bottom) for  $p+\text{Pb}$  collisions at  $\sqrt{s_{NN}} = 115$  GeV. The solid curve in each plot is the central EPS09 NLO result while the dotted curves outline the shadowing uncertainty band.

### B. $J/\psi$ and $\Upsilon(1S)$ production in $\text{Pb}+p$ collisions at $\sqrt{s_{NN}} = 72$ GeV

In this section, the results for  $J/\psi$  and  $\Upsilon$  shadowing in  $\text{Pb}+p$  collisions at  $\sqrt{s_{NN}} = 72$  GeV are presented. Figure 4 shows the results for  $J/\psi$  while Fig. 5 shows the  $\Upsilon$  results. In both cases, the left-hand side shows the ratios  $R_{\text{Pb}p}$  as a function of  $y_{\text{cms}}$  (top) and  $p_T$  in the  $-1.9 < y_{\text{cms}} < -1.4$  rapidity bin (bottom). The rates

to dileptons in the rapidity acceptance, assuming a 1 m long liquid hydrogen target, are shown on the right-hand side of the figures and in the bottom parts of Tables I and II. The lower cross sections at this reduced energy still result in rather high rates for the long liquid hydrogen target, at least at midrapidity.

In these kinematics, the rapidity bin  $-1.9 < y_{\text{cms}} < -1.4$  now corresponds to the more typical fixed-target kinematics with the lead nucleus at lower  $x_1$ . Here the

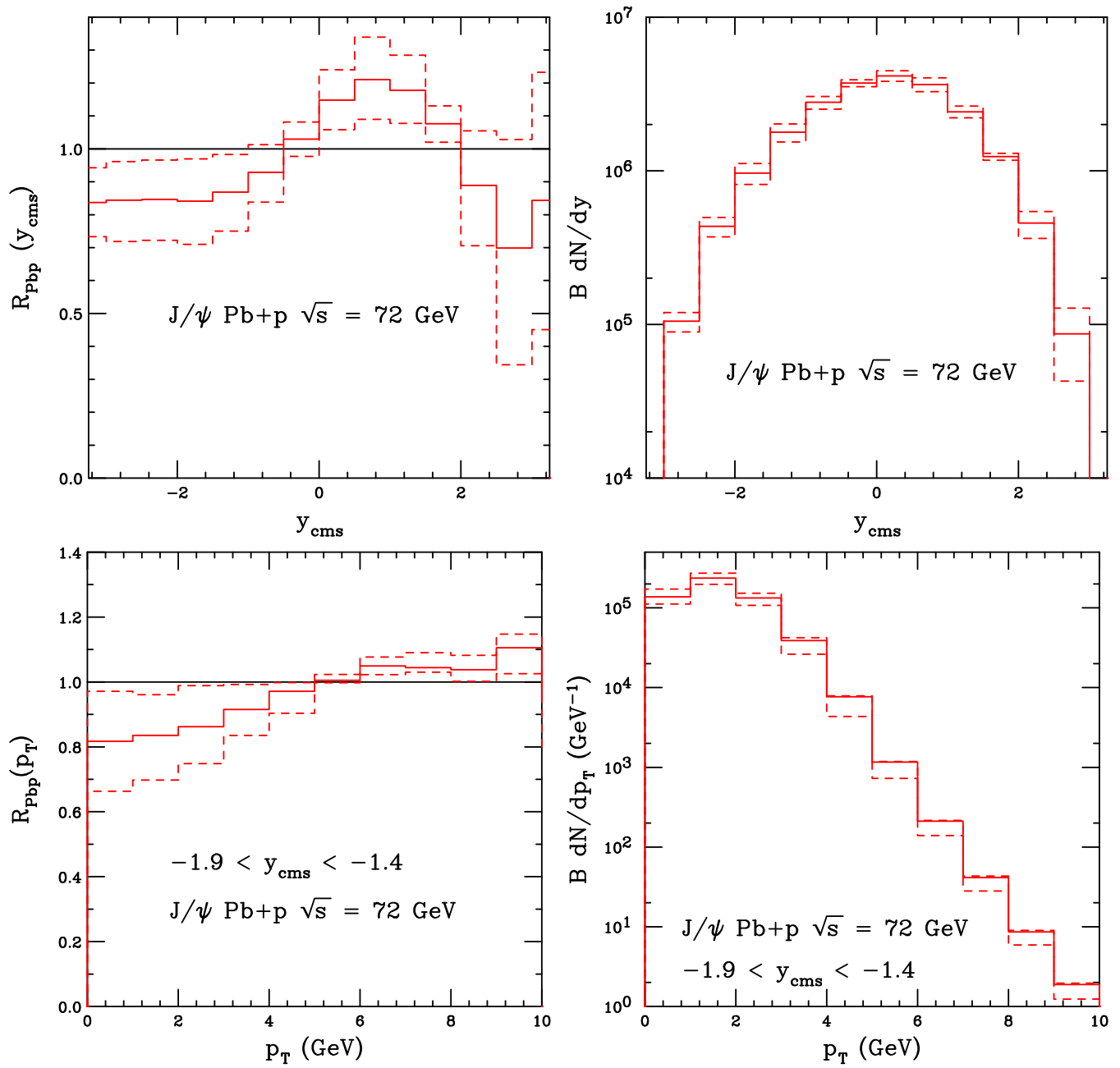


Figure 4: The predicted  $J/\psi$  shadowing ratios (left) and rates (right) as a function of center of mass rapidity (top) and  $p_T$  (bottom) for Pb+p collisions at  $\sqrt{s_{NN}} = 72$  GeV. The solid curve in each plot is the central EPS09 NLO result while the dotted curves outline the shadowing uncertainty band.

ratio  $R_{PbP}(y_{cms})$  is reversed. The  $x$  range for the  $J/\psi$  is in the higher  $x$  end of the shadowing region while the  $\Upsilon$  is just entering the antishadowing region, recall Fig. 1.

The antishadowing peak for  $J/\psi$  in the upper left side of Fig. 4 is actually just at forward rapidity instead of in the  $y_{cms} < 0$  region. (The full center-of-mass rapidity range for  $J/\psi$  production at this energy is  $|y_{cms}| < 3.3$ .) Within the chosen rapidity bin, the  $p_T$ -dependent ratio has the largest uncertainty at low  $p_T$  where there is still

some shadowing. However, at  $p_T > 5$  GeV, the  $x$  values move somewhat into the antishadowing region (lower left panel).

The  $J/\psi$  rates for this system are still high, see the lower half of Table I. Thanks to the length of the H<sub>2</sub> target, for the lead beam the  $p_T$ -integrated rates in this configuration are still on the order of  $10^6$  in the AFTER@LHC acceptance. The  $p_T$ -dependent rates show that the statistics become poor for the  $J/\psi$  at  $p_T > 7$

System	$y_{\text{cms}}$	$N(J/\psi \rightarrow l^+l^-)$	$N(\Upsilon(1S) \rightarrow l^+l^-)$
$p+\text{Pb}$ $\sqrt{s_{NN}} = 115 \text{ GeV}$	-3.75	$2.32 \times 10^5$	-
	-3.25	$1.67 \times 10^7$	-
	-2.75	$9.56 \times 10^7$	-
	-2.25	$2.69 \times 10^8$	$8.68 \times 10^3$
	-1.75	$5.50 \times 10^8$	$1.10 \times 10^5$
	-1.25	$8.88 \times 10^8$	$3.56 \times 10^5$
	-0.75	$1.11 \times 10^9$	$6.81 \times 10^5$
	-0.25	$1.14 \times 10^9$	$9.33 \times 10^5$
	0.25	$1.02 \times 10^9$	$9.47 \times 10^5$
	0.75	$8.36 \times 10^8$	$6.96 \times 10^5$
	1.25	$6.10 \times 10^8$	$3.85 \times 10^5$
	1.75	$3.86 \times 10^8$	$1.39 \times 10^5$
	2.25	$2.10 \times 10^8$	$1.15 \times 10^4$
	2.75	$9.25 \times 10^7$	-
	3.25	$2.04 \times 10^7$	-
3.75	$2.13 \times 10^5$	-	
$\text{Pb}+p$ $\sqrt{s_{NN}} = 72 \text{ GeV}$	-3.25	$1.54 \times 10^3$	-
	-2.75	$1.05 \times 10^5$	-
	-2.25	$4.36 \times 10^5$	-
	-1.75	$9.67 \times 10^5$	$5.36 \times 10^1$
	-1.25	$1.78 \times 10^6$	$5.10 \times 10^2$
	-0.75	$2.79 \times 10^6$	$1.20 \times 10^3$
	-0.25	$3.72 \times 10^6$	$1.66 \times 10^3$
	0.25	$4.15 \times 10^6$	$1.59 \times 10^3$
	0.75	$3.64 \times 10^6$	$1.03 \times 10^3$
	1.25	$2.42 \times 10^6$	$3.78 \times 10^2$
	1.75	$1.24 \times 10^6$	$3.77 \times 10^1$
	2.25	$4.58 \times 10^5$	-
2.75	$8.68 \times 10^4$	-	
3.25	$1.55 \times 10^3$	-	

Table I: The rates per 0.5 unit rapidity for  $J/\psi$  and  $\Upsilon(1S)$  in the two scenarios discussed in the text. The values are given for the EPS09 NLO central set.

GeV. The rates at this energy are helped somewhat since there is antishadowing for  $p_T > 8 \text{ GeV}$  while there is strong shadowing at  $\sqrt{s_{NN}} = 115 \text{ GeV}$ , see Fig. 2.

The situation with  $\Upsilon(1S)$  is similar, see Fig. 5 and Table I. (The rapidity range for  $\Upsilon$  production is  $|y_{\text{cms}}| < 2.4$  so that again the AFTER@LHC acceptance is on the edge of the  $\Upsilon$  range.) The shadowing (or antishadowing) effect is on the order of a few percent. While there are a few thousand  $\Upsilon$  in a year at midrapidity, the rate in the AFTER@LHC acceptance is rather low, under 100 per year, as shown in the lower part of the figure and in Table II. Indeed, there is effectively no rate for the  $\Upsilon$  rate for  $p_T > 4 \text{ GeV}$ .

System	$p_T \text{ (GeV)}$	$N(J/\psi \rightarrow l^+l^-)$	$N(\Upsilon(1S) \rightarrow l^+l^-)$
$p+\text{Pb}$ $\sqrt{s_{NN}} = 115 \text{ GeV}$	0.5	$3.83 \times 10^7$	$1.06 \times 10^3$
	1.5	$6.62 \times 10^7$	$1.79 \times 10^3$
	2.5	$2.83 \times 10^7$	$1.04 \times 10^3$
	3.5	$6.69 \times 10^6$	$3.40 \times 10^2$
	4.5	$9.78 \times 10^5$	$7.93 \times 10^1$
	5.5	$2.03 \times 10^5$	$1.84 \times 10^1$
	6.5	$2.96 \times 10^4$	$4.64 \times 10^0$
	7.5	$6.20 \times 10^3$	$1.62 \times 10^0$
	8.5	$1.12 \times 10^3$	$3.40 \times 10^{-1}$
	9.5	$2.60 \times 10^2$	$6.51 \times 10^{-2}$
	10.5	$3.96 \times 10^1$	$1.03 \times 10^{-2}$
$\text{Pb}+p$ $\sqrt{s_{NN}} = 72 \text{ GeV}$	0.5	$1.38 \times 10^5$	$1.39 \times 10^1$
	1.5	$2.36 \times 10^5$	$2.26 \times 10^1$
	2.5	$1.33 \times 10^5$	$1.20 \times 10^1$
	3.5	$3.90 \times 10^4$	$3.39 \times 10^0$
	4.5	$7.69 \times 10^3$	$7.44 \times 10^{-1}$
	5.5	$1.16 \times 10^3$	$1.71 \times 10^{-1}$
	6.5	$2.11 \times 10^2$	$4.69 \times 10^{-2}$
	7.5	$4.15 \times 10^1$	$1.28 \times 10^{-2}$
	8.5	$8.62 \times 10^0$	$3.25 \times 10^{-3}$
	9.5	$1.89 \times 10^0$	$6.72 \times 10^{-4}$
	10.5	$3.39 \times 10^{-1}$	$1.65 \times 10^{-4}$

Table II: The  $p_T$ -dependent rates per 1 GeV  $p_T$  bin for  $J/\psi$  and  $\Upsilon(1S)$  in the two scenarios discussed in the text. The values are given for the EPS09 NLO central set.

#### IV. CONCLUSIONS

We have only presented a bare minimum of the rates for the breadth of quarkonium studies possible at AFTER@LHC. The fixed-target configuration, especially for long runs with the dedicated proton beam, allows detailed measurements with a range of nuclear targets. We have only shown the Pb results here because the larger nuclear mass number produces what is expected to be the maximum effect due to shadowing.

The large  $x$  region available for nuclear targets in the AFTER@LHC kinematics with a proton beam has the unique capability to make unprecedented studies of this heretofore unexplored range. The AFTER@LHC measurements would bridge the gap between the dedicated fixed-target experiments in the range  $17.2 \leq \sqrt{s_{NN}} \leq 41 \text{ GeV}$  and the d+Au and upcoming  $p+A$  collider experiments at RHIC, albeit in an  $x$  range never before studied.

In the AFTER@LHC configuration with a Pb beam, the rates are smaller, though still significant, and the more conventional  $x$  range is probed.

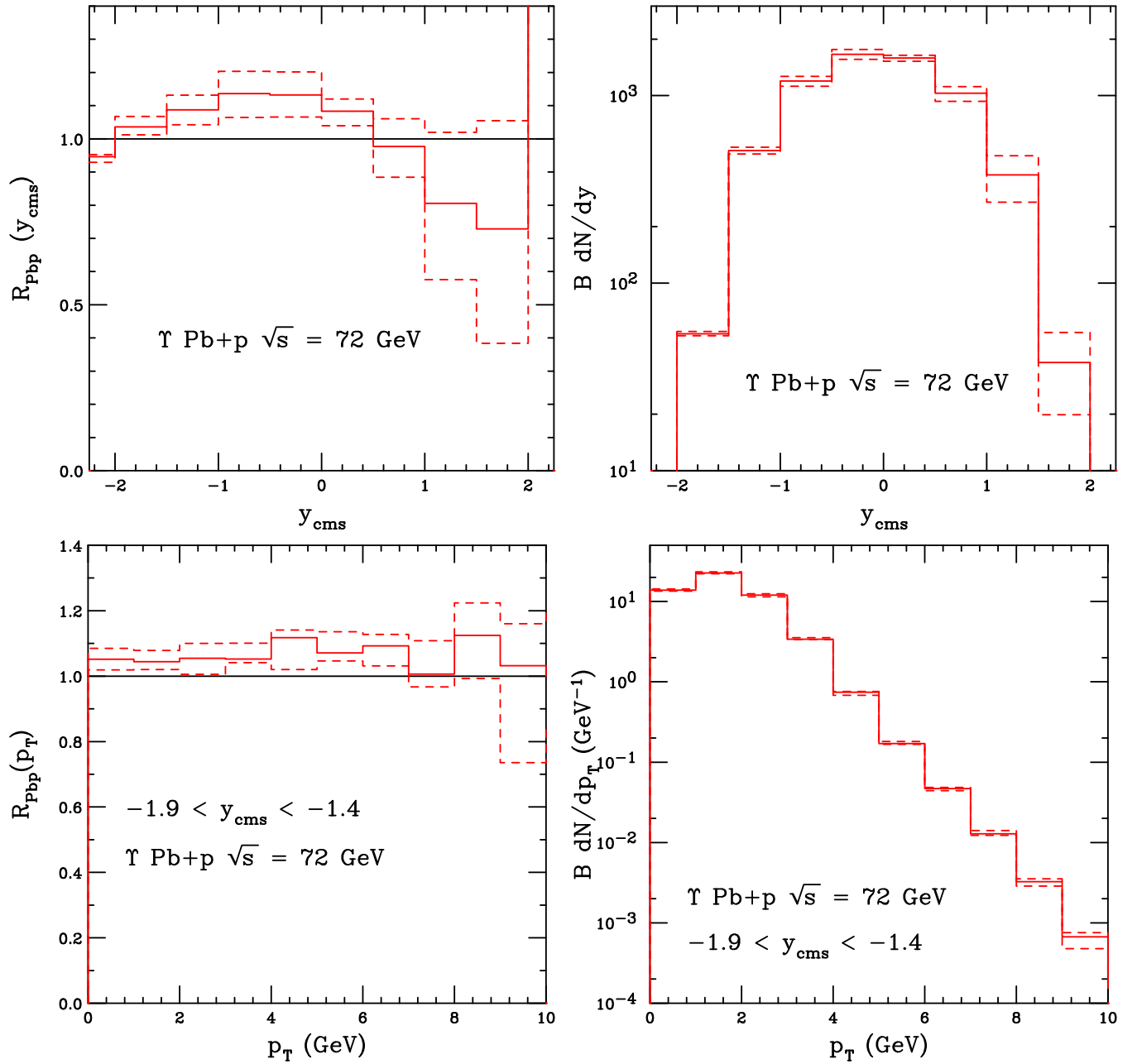


Figure 5: The predicted  $\Upsilon(1S)$  shadowing ratios (left) and rates (right) as a function of center of mass rapidity (top) and  $p_T$  (bottom) for Pb+p collisions at  $\sqrt{s_{NN}} = 72$  GeV. The solid curve in each plot is the central EPS09 NLO result while the dotted curves outline the shadowing uncertainty band.

#### ACKNOWLEDGMENTS

This work was performed under the auspices of the U.S. Department of Energy by Lawrence Livermore National Laboratory under Contract DE-AC52-07NA27344. I also thank the Institute for Nuclear Theory at the University of Washington, where this work was initiated, for hospitality.

- 
- [1] S. J. Brodsky, F. Fleuret, C. Hadjidakis and J. P. Lansberg, Phys. Rept. **522** (2013) 239.
- [2] R. Gavai, D. Kharzeev, H. Satz, G. A. Schuler, K. Sridhar and R. Vogt, Int. J. Mod. Phys. A **10** (1995) 3043.
- [3] K. J. Eskola, H. Paukkunen and C. A. Salgado, JHEP **0904** (2009) 065.
- [4] J. Pumplin, D. R. Stump, J. Huston, H. L. Lai, P. M. Nadolsky and W. K. Tung, JHEP **0207** (2002) 012; D. Stump, J. Huston, J. Pumplin, W. K. Tung, H. L. Lai, S. Kuhlmann and J. F. Owens, JHEP **0310**(2003) 046.
- [5] R. E. Nelson, R. Vogt and A. D. Frawley, Phys. Rev. C **87** (2013) 014908.
- [6] R. E. Nelson, R. Vogt and A. D. Frawley, in preparation.
- [7] H. L. Lai, M. Guzzi, J. Huston, Z. Li, P. Nadolsky, J. Pumplin, C.-P. Yuan, Phys. Rev. D **82** (2010) 074024.
- [8] R. Vogt, in preparation.
- [9] M. Arneodo *et al.* [European Muon Collaboration], Phys. Lett. B **211** (1988) 493; J. Ashman *et al.* [European Muon Collaboration], Phys. Lett. B **202** (1988) 603.
- [10] L. W. Whitlow, E. M. Riordan, S. Dasu, S. Rock and A. Bodek, Phys. Lett. B **282**, 475 (1992).
- [11] M. C. Abreu *et al.* [NA38 Collaboration], Phys. Lett. B **444** (1998) 516.
- [12] B. Alessandro *et al.* [NA50 Collaboration], Eur. Phys. J. C **33** (2004) 31.
- [13] M. J. Leitch *et al.* [E866 Collaboration], Phys. Rev. Lett. **84** (2000) 3256.
- [14] I. Abt *et al.* [HERA-B Collaboration], Phys. Lett. B **638** (2006) 407.
- [15] R. Vogt, Phys. Rev. C **61** (2000) 035203.
- [16] K. J. Eskola, V. J. Kolhinen and P. V. Ruuskanen, Nucl. Phys. B **535** (1998) 351.
- [17] K. J. Eskola, V. J. Kolhinen and C. A. Salgado, Eur. Phys. J. C **9** (1999) 61.
- [18] C. Lourenço, R. Vogt and H. Wöhri, JHEP **0902** (2009) 014.
- [19] F. Arleo and S. Peigné, JHEP **1303** (2013) 122; F. Arleo, R. Kolevator, S. Peigné and M. Rustomova, JHEP **1305** (2013) 155.
- [20] D. C. McGlinchey, A. D. Frawley and R. Vogt, Phys. Rev. C **87** (2013) 054910.
- [21] V. D. Barger, W. Y. Keung and R. J. Phillips, Phys. Lett. B **91** (1980) 253.
- [22] V. D. Barger, W. Y. Keung and R. J. Phillips, Z. Phys. C **6** (1980) 169.
- [23] M. L. Mangano, P. Nason, and G. Ridolfi, Nucl. Phys. B **373** (1992) 295.
- [24] G. A. Schuler and R. Vogt, Phys. Lett. B **387** (1996) 181.
- [25] M. L. Mangano, P. Nason, and G. Ridolfi, Nucl. Phys. B **405** (1993) 507.